

Eigenvalue spectral properties of sparse random matrices for neural networks obeying Dale's law.

Isabelle D Harris^{1,2,3}, Hamish Meffin^{1,4}, Anthony N Burkitt¹, and Andre D.H Peterson^{1,2,3}

¹Department of Biomedical Engineering, University of Melbourne.

²Graeme Clark Institute, University of Melbourne

³Department of Medicine, St. Vincent's Hospital, University of Melbourne

⁴National Vision Research Institute, Australian College of Optometry, Melbourne

Abstract

This work examines the relationship between sparse random network architectures and neural network dynamics. Specifically, we examine the impact of sparse connectivity combined with Dale's law on network stability by analysing the eigenspectrum of the networked Jacobian. We define α as the probability that a neuron is connected to another neuron, and consider all levels of network sparseness ($0 \leq \alpha \leq 1$). Previous work has examined the effects of Dale's law for fully connected random matrices that are balanced (zero mean) [30] or unbalanced [15] and sparse networks ($\alpha \ll 1$) with constant weights for each population [26, 22]. Our work significantly extends these results by incorporating both sparsity and Dale's law into both balanced and unbalanced matrices with random weights. We find that the stability and density of the eigenspectrum becomes nonlinearly dependent on the sparsity, population means and variances of the weights and give explicit formulae describing this.

Contrary to the balanced, single population case where the sparsity linearly scales the eigenspectrum [37], we find for unbalanced, single populations and (un)balanced two population cases, the sparsity scales the eigenspectrum nonlinearly. This happens for all cases above except when both population means are zero, which is equivalent to the balanced, single population case. Further, we show that the eigenspectral density becomes non-uniform for the above cases which extends previous results, which only required the population variances to be different. We give an explicit formula for the spectral density when sparsity is introduced with Dale's law: the spectral radius and density has a nonlinear dependence on the population means, variances and sparsity parameter for both the balanced and unbalanced cases. We deduce new analytical formulas for the eigenspectral radius and outlier, which explicitly describes how these properties nonlinearly change as functions of the sparsity parameter, the individual population means and variances. Sparsity and Dale's law are fundamental anatomical properties of biological neural networks, and by quantifying the effects of these properties on the Jacobian's eigenspectra, we gain insight into how network structure influences system stability, state transitions and neural network behaviour.

1 Introduction

Understanding the spatio-temporal dynamics of large populations of neurons in the cortex is a fundamentally difficult open problem in both theoretical and experimental neuroscience, particularly the relationship between network connectivity and dynamics. Theoretically, this has been typically studied by either averaging over the synaptic connection weights, thereby sacrificing network structure, or via large-scale numerical simulations of neural models that are mathematically intractable. An effective approach that preserves the statistical structure of the synaptic connectivity whilst still being mathematical feasible is to study the dynamics of partially random networks of neurons. Network dynamics in this framework are examined through changes in the eigenvalue spectral distribution of the network Jacobian, which is a function of the synaptic connectivity matrix [30]. This paper mathematically examines the stability properties of the Jacobian's eigenspectrum when more realistic anatomical structure is incorporated into the connectivity matrix, such as sparsity, network (im)balance, and Dale's law.

A key feature of biological neural networks is that they are not fully-connected, namely neurons do not receive input from every other neuron in the network [7, 4, 12]. Usually the number of connections is relatively small, but varies depending on spatial scale, location, network size, and specific population wiring related to function. We introduce sparsity into the synaptic connectivity matrix by defining a sparsity parameter, α , as the probability that a neuron is connected to another neuron, so that $\alpha=1$, denotes a fully connected network. Previous analyses only considered fully connected networks [30, 35, 19, 15], or sparse networks with constant weights describing each of the excitatory and inhibitory populations [26, 22, 14], or sparse one population random networks [37, 14]. Furthermore, these works [26, 22] are only valid in the very sparse limit, i.e., $\alpha \ll 1$. This paper generalises the previous results to include all levels of sparsity $0 \leq \alpha \leq 1$ in two-population networks with differently distributed weights and different network (im)balances.

There is a considerable amount of experimental [4, 21, 13] and theoretical [39, 7, 8, 34] evidence that strongly suggests that brain activity crucially depends on the dynamic balance between excitation and inhibition, and is essential for brain function [4, 19]. Many anatomical and physiological network properties adjust homeostatically to

maintain balanced E-I input [20], and network imbalances can lead to pathological brain dynamics, such as epileptic seizures [15]. However, the concept of network balance is ambiguous [1] and needs to be defined carefully. Functional network balance is a dynamical property that changes depending on the network activity. Specifically, we define functional network balance as the sum of synaptic inputs, i.e., the weights multiplied by the firing rates [24, 7]. However, in this work we do not consider the firing rates, and focus instead on structural network balance. Structural network balance in biological neural networks is intrinsically tied to Dale's law, where neurons in the cortex are either excitatory (E) or inhibitory (I) in their action on target neurons [10]. Dale's law introduces a macroscopic anatomical constraint upon the random synaptic connectivity matrix; i.e. a partially random neural network. Therefore, we define structural E-I network balance to be the network state in which the mean excitatory (E) weights equals the mean magnitude of the inhibitory (I) weights [4, 7, 24]. We examine both structurally balanced and unbalanced networks in combination with sparsity in this framework to understand their impacts on brain dynamics, particularly state transitions to physiologically realistic asynchronous activity [26].

In this paper, we consider the combined effects of incorporating sparsity and Dale's law into a random neural network. In particular, we pose the question: how does incorporating both sparsity and Dale's law into the connectivity matrix affect the stability and density of the eigenspectrum? We answer this by carefully analysing the eigenvalue distribution of the network Jacobian for sparse balanced and unbalanced random synaptic connectivity matrices obeying Dale's law. Specifically, we deduce a number of mathematically explicit formulas that extend previous analyses [30, 15, 14], yielding a quantitative relationship between sparsity, the E-I populations statistics and principal properties of the eigenspectrum.

2 Network model and analysis

In this study the neural network dynamics are described by

$$\dot{x}_i(t) = -\frac{x_i(t)}{\tau} + \sum_{j=1}^N w_{ij}\phi(x_j(t)), \quad (1)$$

where $x_i(t)$ is the membrane potential of the i th neural unit, τ is the passive membrane time constant, w_{ij} is an entry in a $N \times N$ partially random network connectivity matrix W , $\phi(x_i(t))$ is an activity-to-firing rate coupling function. The function ϕ is defined as a real valued, bounded, smooth, and strictly monotonically increasing odd function on the infinite domain with $\phi(0) = 0$, $\phi'(0) = 1$, and $\phi \rightarrow \pm 1$ for $x \rightarrow \pm\infty$, e.g., $\phi(x) = \tanh(x)$ [33, 35, 26, 15]. For such a function, the system yields both positive and negative outputs. This can be interpreted as a firing rate where ϕ is the deviation of the output away from a homogeneous average or baseline rate for the network, which can be considered as the homeostatic fixed point of the network dynamics, and $\phi(-\infty)$ is the zero-point of the firing rate scale. All terms in Eq. 1 have units of volts per unit time, $[V][t]^{-1}$.

The equilibria of this network model are the solutions of the expression

$$\mathbf{x}^* = \tau W \phi(\mathbf{x}^*), \quad (2)$$

where $\mathbf{x}^*, \phi(\mathbf{x}^*) \in \mathbb{R}^N$. Calculating the solutions of Eq. 2 for large neural networks is typically both mathematically intractable and computationally infeasible, since the number of equilibria scales exponentially with system size [15, 40]. Neural networks that are described by a random connectivity matrix with zero mean always yield a 'trivial' homogeneous equilibrium solution that represents a stable fixed point of the network dynamics with homogeneous non-zero firing rate. However, the existence of a homogeneous equilibrium solution for structurally (E-I) balanced and unbalanced random networks obeying Dale's law requires that the sum of the rows of the connectivity matrix is equal for all rows [15]. The row-sum condition is satisfied when

$$\sum_j^N w_{ij} = N\mu_r, \quad (3)$$

where μ_r is the average connectivity weight. If Eq. 3 is satisfied, there exists a homogeneous equilibrium solution when $x_k^* = x_0^*$ for all units k provided that

$$x_0^* = \tau N \mu_r \phi(x_0^*), \quad (4)$$

has a solution for all $k \in [1, N]$. Structural (E-I) balance or imbalance is defined as the weighted contributions of the average neural population strengths. Therefore the expected value of the entries of the rows of W , namely the value of μ_r , indicates whether the network is balanced. If the connectivity matrix is excitatory dominated then $\mu_r > 0$, or inhibitory dominated $\mu_r < 0$, and it is structurally E-I balanced when $\mu_r = 0$.

Networks that satisfy the row-sum condition and structural (E-I) balance, permit a 'trivial' homogeneous equilibrium solution, $\mathbf{x}_0^* = \mathbf{0}$, as described above. If a network satisfies the row-sum condition, but is structurally E-I unbalanced, a constant homogeneous equilibrium solution exists, $\mathbf{x}_0^* = \boldsymbol{\xi}$. Alternatively, if the row-sum condition is not satisfied and the network is structurally E-I unbalanced, then the system permits heterogeneous equilibria, i.e., different neurons i attain two or more different equilibrium values. Heterogeneous equilibrium solutions \mathbf{x}^* are difficult to calculate, and are dependent on the individual realisation of the connectivity matrix [23].

To evaluate the local stability of the system around the equilibria, we study the eigenspectrum of the networked Jacobian.

$$\mathcal{J}(\mathbf{x}^*) = \left[-\frac{1}{\tau} \mathbb{1}_N + W \Phi'(\mathbf{x}^*) \right], \quad (5)$$

where, $\mathbb{1}_N$ is the identity matrix, and $\Phi'(\mathbf{x}^*)$ is an $N \times N$ diagonal matrix with diagonal entries

$$\frac{\partial \phi(x_j)}{\partial x_j} \Big|_{\mathbf{x}^*} = \phi'(x_j^*). \quad (6)$$

When the real part of at least one of the eigenvalues of the Jacobian, Eq. 5, becomes positive, the fixed point becomes unstable and spontaneous dynamics emerge [2, 22]. Therefore, the stability and neural dynamics is influenced by the eigenspectrum of the Jacobian, which from random matrix theory, depends on the statistical structure of the synaptic connectivity matrix W .

If the homogeneous equilibria is the ‘trivial’ zero solution, $\mathbf{x}_0^* = \mathbf{0}$, then the matrix $\Phi'(\mathbf{x}_0^*) = \mathbb{1}_N$ since $\phi'(0) = 1$. Thus, the eigenspectrum of the Jacobian depends only on the synaptic connectivity matrix W with diagonal offset of $-1/\tau$. However, if the homogeneous equilibria is a constant value, ξ for all units i , $\mathbf{x}_0^* = \xi$, the matrix $\Phi'(\mathbf{x}^*) = \gamma \mathbb{1}_N$ since $\phi'(\xi) = \gamma$. This introduces an additional dependence in the Jacobian, which takes the form $\mathcal{J}(\mathbf{x}^*) = \left[-\frac{1}{\tau} \mathbb{1}_N + \gamma W \right]$. Since γ exclusively scales the entries in W , the strength of the entries in W changes, but the inherent statistical structure of \mathcal{J} remains unchanged. Since our analysis focuses on examining the effects of implementing anatomically realistic structure into a random connectivity matrix, namely Dale’s law, structural E-I imbalance, and sparsity, we assume unit scaling factor $\phi'(0) = 1$, and examine the eigenspectrum of

$$\mathcal{J}(\mathbf{x}_0^*) = \left[-\frac{1}{\tau} \mathbb{1}_N + W \right]. \quad (7)$$

The network Jacobian for heterogeneous equilibrium solutions incorporates an additional (nested) dependence of the connectivity matrix through the term $\Phi'(\mathbf{x}^*)$. To examine the influence of the statistical structure of the connectivity matrix W on the eigenvalues of the Jacobian, and hence the network dynamics, mean-field techniques are required [23]. This analysis which is outside the scope of this investigation.

3 Eigenvalue spectral properties of synaptic connectivity matrices

To investigate the impact of Dale’s law, structural E-I imbalance, and sparsity in random neural networks obeying Dale’s law, we analyse the changes in the eigenspectral distribution of the network Jacobian, Eq. 7. We use the following key results from random matrix theory to examine this relationship.

3.1 Eigenvalues of a random matrix

The elements in large synaptic connectivity matrices are sampled randomly from a Gaussian or any identically independent distribution. Therefore, we use results from random matrix theory in this investigation [30, 15]. A central result of random matrix theory is Girko’s circular law. This law states that the empirical spectral distribution of a random matrix, A , with entries a_{ij} independently and identically distributed (iid) with mean $\mu = 0$, variance $\sigma^2 = \frac{1}{N}$, converges to the unit disc on the complex plane [25, 11, 30, 37, 38]. A secondary result states that an eigenvalue outlier escapes the eigenspectral-disc if A has nonzero mean [36]. Consequently an iid random matrix A_N with mean $\mu \neq 0$, variance $\sigma^2 = \frac{1}{N}$, and finite fourth moment has an eigenspectrum with a central eigenspectral-disc, with radius $\mathcal{R} = \sigma\sqrt{N}$, and a single eigenvalue outlier, λ_O , that escapes to the point $\lambda_O = \mu N$ on the complex plane.

3.2 Eigenvalues of sparse random matrices

A sparse random matrix, W , is characterised by three statistics; the probability of a nonzero element α , the mean μ , and variance σ^2 of the nonzero entries. We construct our connectivity matrix W by combining sparse, random and deterministic components as per Eq.(8) below. AD is the random component, and M is a low-rank deterministic component. Incorporating network sparsity is achieved by a Hadamard (element-wise) product of the Gaussian component $AD + M$ with a Boolean random matrix S . A sparse random matrix is defined as,

$$W = S \circ (AD + M), \quad (8)$$

where S is an iid Boolean random matrix with probability α of an element being non-zero, \circ is the element wise product, A is an iid random matrix with zero mean and unit variance, D is a diagonal matrix of standard deviations, $D = \text{diag}(\sigma, \dots, \sigma)$, $M = \mathbf{u}\mathbf{v}^\top$ is a rank one matrix perturbation with row vectors $\mathbf{u} = (1, \dots, 1)^\top$, $\mathbf{v} = (\mu, \dots, \mu)^\top$. If $\mu \neq 0$ then the connectivity matrix W is structurally (E-I) unbalanced.

We scale the mean and standard deviation, by \sqrt{N} to ensure that the properties of the eigenvalue spectrum are as independent as possible from the system size. Specifically, we use scaled variables $\tilde{\mu} = \frac{\mu}{\sqrt{N}}$, and $\tilde{\sigma} = \frac{\sigma}{\sqrt{N}}$.

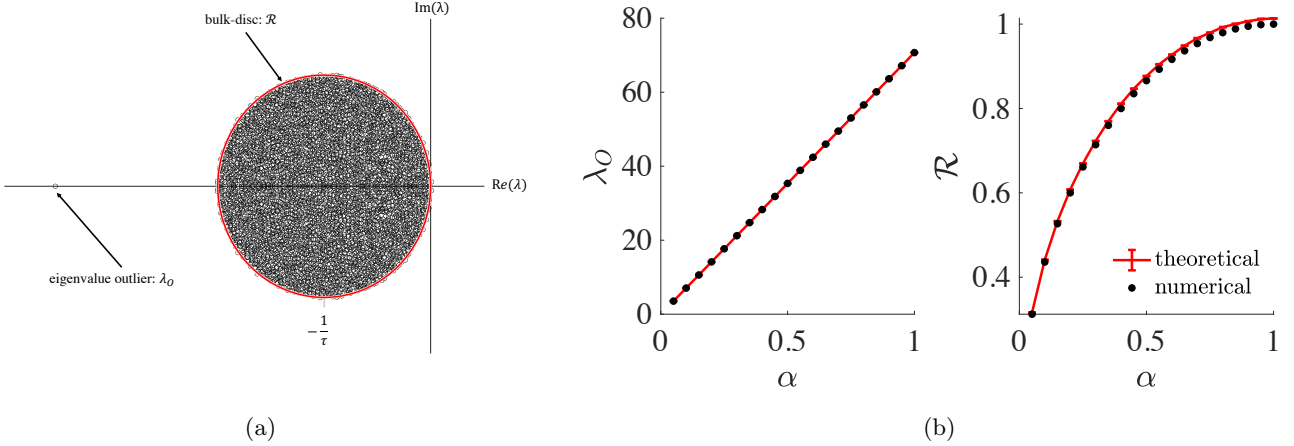


Figure 1: (a) An eigenspectrum with $N = 5000$, $\tilde{\sigma} = \frac{1}{\sqrt{N}}$, $\tilde{\sigma} = \frac{1}{\sqrt{N}}$, $\alpha = 0.99$. (b) The eigenvalue outlier location and radius of the eigenspectral-disc for the matrix defined in Eq. 8, as a function of the sparsity parameter α . The theoretical location and radius is shown in black and was calculated using Eq. 10 and 12, respectively. The average largest λ_O and second largest eigenvalues λ_1 over the realisations is shown in red. W was constructed for 100 realisations and has size $N = 5000$, mean $\tilde{\sigma} = \frac{1}{\sqrt{N}}$, and standard deviation $\tilde{\sigma} = \frac{1}{\sqrt{N}}$.

A typical eigenspectrum for an structurally E-I imbalanced matrix W is illustrated in Figure 1(a). The two primary properties are the location of the eigenvalue outlier, λ_O , and the radius of the eigenspectral-disc, \mathcal{R} . Results from random matrix theory predict that $\lambda_O = \mathbb{E}(w_{ij})N$, and $\mathcal{R} = \sqrt{\text{Var}(w_{ij})N}$ [37, 38, 36, 30, 25]. However, these results are only explicitly proven for fully connected networks with nonzero mean, and sparse random matrices with zero mean.

We build on these previous results to predict the location of $\lambda_O = \mathbb{E}(w_{ij})N$, and the radius $\mathcal{R} = \sqrt{\text{Var}(w_{ij})N}$ for sparse unbalanced random connectivity matrices. For sparse random matrices that obey Dale's law, we derive expressions for λ_O , and \mathcal{R} , by first deriving expressions for the means and variances of the weights w_{ij} .

We relate (Appendix 5.1) the mean of the weights, $\mathbb{E}(w_{ij})$, to the normalised mean $\tilde{\mu}$, and sparsity parameter α , by

$$\mathbb{E}(w_{ij}) = \alpha\tilde{\mu}. \quad (9)$$

Therefore, we predict that the location of the eigenvalue outlier is given by

$$\lambda_O = \alpha\tilde{\mu}N. \quad (10)$$

We compare the predicted eigenvalue outlier defined in Eq. 10 to the eigenvalue outlier in the numerical eigenspectrum of sparse random matrices constructed using Eq. 8. Numerical eigenspectra are calculated using MATLAB, and this is performed for a large number of realisations of the sparse random matrix. We compute the eigenvalue with the largest magnitude for each realisation, and average the eigenvalue-outliers over all realisations to obtain a numerical estimate for λ_O . The predicted eigenvalue outlier and average numerical eigenvalue outlier over 100 realisations of the matrix W is illustrated in Figure 1(b).

To calculate the radius of the eigenspectral disc, the variance of the weights, $\text{Var}(w_{ij}) = \mathbb{E}(w_{ij}^2) - \mathbb{E}(w_{ij})^2$ is derived as a function of the three primary statistics; the normalised mean $\tilde{\mu}$, the normalised standard deviation $\tilde{\sigma}$, and sparsity parameter α , see Appendix 5.1 for details. The expression for the variance is now dependent on both the mean and sparsity parameters,

$$\text{Var}(w_{ij}) = \alpha(1 - \alpha)\tilde{\mu}^2 + \alpha\tilde{\sigma}^2. \quad (11)$$

Therefore, we can now compute the radius of the eigenspectral-disc as

$$\mathcal{R} = \sqrt{N[\alpha(1 - \alpha)\tilde{\mu}^2 + \alpha\tilde{\sigma}^2]}. \quad (12)$$

It is clear from the expressions in Eq. 10 and Eq. 12 that the normalised scaling ensures that the eigenvalue outlier location is of order $O(\sqrt{N})$ and the radius of order $O(1)$ as N gets large. From this point, our analysis implicitly assumes this respective scaling.

This choice of scaling is justified by our focus on balanced or inhibitory dominated networks that are close to balanced as opposed to excitatory dominated. In excitatory dominated networks, the eigenvalue outlier lies to the right of the disc and causes network activity to diverge and saturate to the upper bound of the firing rate function as the system size increases ($O(\sqrt{N})$). This activity is not of interest from a physiological perspective as it does not generate the spontaneous asynchronous activity associated with normal brain function, for example, the resting state [26, 22, 19]. Non-trivial spontaneous behaviour only emerges when the eigenspectral-disc crosses the imaginary axis and the network activity becomes unstable but not divergent. For this to occur, the network must be either balanced

or inhibitory dominant so that the radius of the eigenspectral disc can grow with the variance of the connectivity matrix.

Previous work on sparse random matrices with zero mean [37] finds that the radius of the eigenspectral-disc scales linearly with the sparsity and the variance. By comparison, when the mean is non-zero, we find the radius is dependent on all three statistics $\tilde{\mu}$, $\tilde{\sigma}$, α and the system size N . Figure 1 illustrates the predicted expression in Eq. 12 and the numerically calculated average radius of the eigenspectral-disc. To calculate the average radius, we extract the eigenvalue with the second largest magnitude for each realisation, and then average these values over all realisations. Based on results from random matrix theory, we know that the eigenvalue with the second largest magnitude should lie exactly on, or just within the radius of the eigenspectral disc [37, 37]. We find that there is an agreement between the predicted eigenvalue outlier and radius and the numerical estimates of the eigenvalue outlier and radius, and the relative error between the estimates is of the order 10^{-4} .

3.3 Eigenspectral properties of sparse random matrices that obey Dale's law

Distinct neural populations (Dale's law) are incorporated into the synaptic connectivity matrix by specifying two separate but related Gaussian distributions for each of the excitatory and inhibitory populations. The sparse random matrix is partitioned into an excitatory partition $(\tilde{\mu}_e, \tilde{\sigma}_e^2)$ and an inhibitory partition $(\tilde{\mu}_i, \tilde{\sigma}_i^2)$. The synaptic connectivity matrix still takes the form of Eq.(8), where S , and A are defined as before. However, D is now a diagonal matrix of excitatory and inhibitory variances,

$$D = \text{diag}(\underbrace{\tilde{\sigma}_e, \dots, \tilde{\sigma}_e}_{Nf \text{ times}}, \underbrace{\tilde{\sigma}_i, \dots, \tilde{\sigma}_i}_{N(1-f) \text{ times}}), \quad (13)$$

and the perturbation $M = uv^\top$ is an outerproduct matrix of population means, with

$$, u = (1, \dots, 1)^\top, \quad v = (\underbrace{\tilde{\mu}_e, \dots, \tilde{\mu}_e}_{Nf \text{ times}}, \underbrace{\tilde{\mu}_i, \dots, \tilde{\mu}_i}_{N(1-f) \text{ times}})^\top. \quad (14)$$

The matrix M consists of Nf columns with identical entries $\tilde{\mu}_e$ and the remaining $N(1-f)$ columns with entries $\tilde{\mu}_i$. Here, structural (E-I) balance is defined in terms of the combined relative contributions of the excitatory and inhibitory neurons, i.e., the expected value of the entries, $\mathbb{E}(w_{ij})$. We exploit this formalism to examine sparse structurally (E-I) unbalanced synaptic connectivity matrices, $\mathbb{E}(w_{ij}) \neq 0$, and refer to these networks as sparse unbalanced random networks obeying Dale's law.

A typical eigenspectrum for a sparse unbalanced random matrix W that obeys Dale's law is illustrated in Figure 2(a). This figure illustrates the eigenvalue outlier, λ_O , and the radius of the eigenspectral-disc, \mathcal{R} , as the two primary properties of the eigenspectral distribution. These properties are hypothesised to be defined by $\lambda_O = \mathbb{E}(w_{ij})N$, and $\mathcal{R} = \sqrt{\text{Var}(w_{ij})N}$ [30, 37, 36].

We commence as before by deriving expressions for the mean and variance of the weights w_{ij} in W , where W is defined by Eq. 8. The mean and variance are given by,

$$\mathbb{E}(W) = f\mu_{se} + (1-f)\mu_{si}, \quad (15)$$

$$\text{Var}(W) = f\sigma_{se}^2 + (1-f)\sigma_{si}^2, \quad (16)$$

where

$$\mu_{sk} = \alpha\tilde{\mu}_k \quad (17)$$

$$\sigma_{sk}^2 = \alpha(1-\alpha)\tilde{\mu}_k^2 + \alpha\tilde{\sigma}_k^2 \quad (18)$$

are the means and variances of the excitatory and inhibitory weights ($k = e, i$) derived in Appendix 5.2.

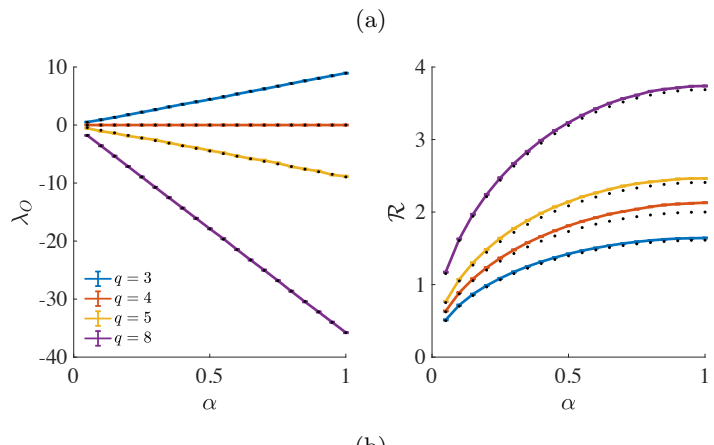
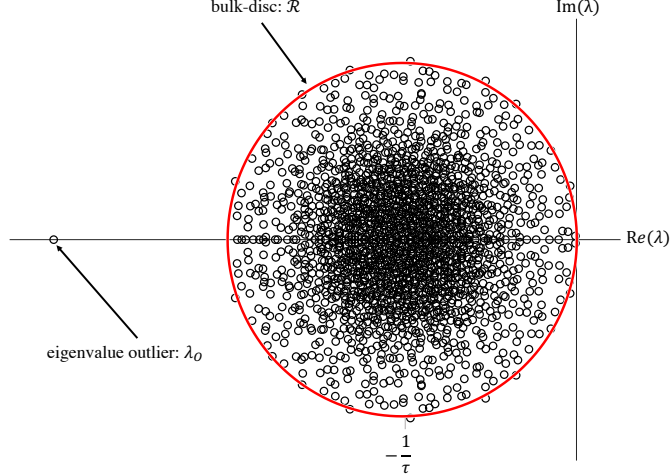
Therefore, the location of the eigenvalue-outlier, and radius of the central eigenspectral-disc for sparse unbalanced random matrices that obey Dale's law take the values,

$$\lambda_O = N[f\mu_{se} + (1-f)\mu_{si}]. \quad (19)$$

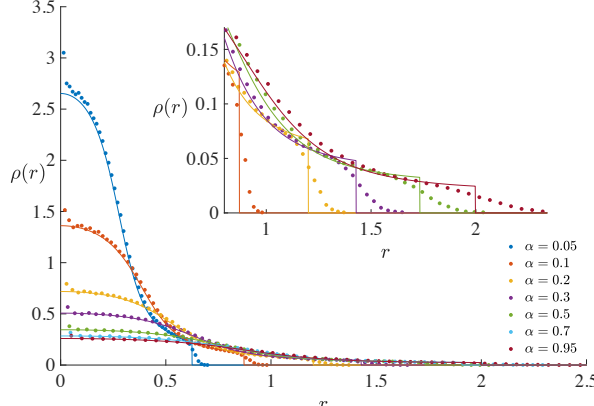
$$\mathcal{R} = \sqrt{N[f\sigma_{se}^2 + (1-f)\sigma_{si}^2]}. \quad (20)$$

We compare our theoretical eigenvalue outlier values and radii to numerical eigenspectra of sparse random matrices constructed using Eq. 8. This comparison of the eigenvalue outlier values and the radius of the central eigenspectrum disc is illustrated in Figure 2(b). The predicted eigenvalue outlier location and radius of eigenspectral-disc radius have an excellent agreement with the numerically calculated eigenvalue outlier and radius of the eigenspectral-disc.

We observe that sparsity appears linearly in the expression for the degree of structural E-I balance, and hence the eigenvalue outlier, Eq. 19. Additionally, the radius of the eigenspectral disc is non-linearly dependent on the sparsity parameter, α , the normalised population means $\tilde{\mu}_e, \tilde{\mu}_i$, and normalised population variances $\tilde{\sigma}_e^2, \tilde{\sigma}_i^2$. From Eq. 20 we see that when the connectivity is fully connected $\alpha = 1$, the radius depends only on the population variances, a result consistent with [30, 36, 15]. However, once sparsity is introduced into the connectivity, $0 < \alpha < 1$, the eigenspectral disc radius changes as a function of all population statistics $(\alpha, \mu_k, \sigma_k^2)$.



(b)



(c)

Figure 2: (a) An eigenvalue spectrum with parameters: $N = 2000, f = 0.8, \mu_e = \frac{1}{\sqrt{N}}, \sigma_e = \frac{1}{\sqrt{N}}, \mu_i = -\frac{4.7}{\sqrt{N}}, \sigma_i = \frac{4.7}{\sqrt{N}}, \tau = 1, \zeta = 1, \alpha = 0.99$. (b) The eigenvalue outlier location and radius of the eigenspectral-disc for the matrix defined in Eq. 8, as a function of the sparsity probability α . The theoretical outlier location and radius (blue, orange, yellow, purple) were calculated using definitions in Eq. 19 and 20, respectively. The orange line represents the case when the outlier is zero and there is structural E-I balance, i.e., $q = 4$ and $f = 0.8$ ensures that Eq. 19 gives zero. The largest λ_o and second largest eigenvalues λ_1 averaged over 100 realisations is shown in black. Parameters of W are $N = 2000, f = 0.8, \mu_e = \frac{1}{\sqrt{N}}, \mu_i = -\frac{4}{\sqrt{N}}, \sigma_e = \frac{1}{\sqrt{N}}, \sigma_i = \frac{4}{\sqrt{N}}, f = 0.8$, and (blue) $q = 3$, (orange) $q = 4$, (yellow) $q = 5$, and (purple) $q = 8$. (c) Non-uniform spectral density curves as a function of disc radius and sparsity parameter α with analytical expression as solid lines and points are average density over 500 realisations. Parameters of W are $N = 2000, \mu_e = \frac{1}{\sqrt{N}}, \mu_i = -\frac{4}{\sqrt{N}}, \sigma_e = \frac{1}{\sqrt{N}}, \sigma_i = \frac{4}{\sqrt{N}}$, and $f = 0.8$.

3.3.1 Non-uniform spectral density of eigenvalue distribution

Previous studies [30, 36, 15] have shown that a difference in the variances of the excitatory and inhibitory weights, σ_e^2, σ_i^2 , cause the density of the eigenvalue distribution to be non-uniform. We extend these results to the sparse case and show that it is the difference in variances of the sparsely connected excitatory and inhibitory weights, $\sigma_{se}^2, \sigma_{si}^2$ that causes the density to be non-uniform. This phenomena is observed in Figure-2(a & c).

The central result of [30] is the derivation of the expression of the non-uniform eigenspectral density for connectivity matrices obeying Dale's law. The density is a function of the distance to the centre of the disc on the complex plane, $|z|$, and the expression was simplified further in [15]. We incorporate our expressions for the sparse neural population variances, Eq. 18 into the spectral density expression defined in [15].

The global spectral density for a sparse (un)balanced random connectivity matrix obeying Dale's law is;

$$\rho_{RA}(z) = \begin{cases} \frac{1}{\pi N \sigma_{si}^2} \left[1 - \frac{g}{2} \mathcal{H}_f \left(g \frac{|z|^2}{N \sigma_{si}^2} \right) \right] & |z| \leq \mathcal{R} \\ 0 & |z| > \mathcal{R} \end{cases} \quad (21)$$

with

$$g = 1 - \sigma_{si}^2 / \sigma_{se}^2 = 1 - \frac{(1-\alpha)\mu_i^2 + \sigma_i^2}{(1-\alpha)\mu_e^2 + \sigma_e^2}. \quad (22)$$

and

$$\mathcal{H}_f(x) = \frac{2f - 1 + x}{\sqrt{1 + x(4f - 2 + x)}} + 1. \quad (23)$$

By symmetry an equivalent expression holds for σ_{si}^2 and σ_{se}^2 interchanged in Eq. 21 and Eq. 22, with $2f - 1$ replaced by $1 - 2f$ in Eq. 23. Note that the conditions on σ_{sk}^2 for $k = e, i$, and g stated in [15] are not required, as the symmetrical expressions yield the equivalent outputs regardless whether these conditions are met.

Using this expression, the spectral density curves for a sparse balanced and unbalanced random connectivity matrices obeying Dale's law are calculated and compared with numerically simulated density curves for the same parameters. The agreement between the analytical expression and the numerical simulation is illustrated in Figure 2(c). As expected, the results indicate that the spectral density curves are dependent on the variances of the sparse excitatory and inhibitory weights σ_{si}^2 and σ_{se}^2 . Consequently, the density curves are dependent on the sparsity parameter α , the population means μ_e, μ_i , and population variances σ_e^2, σ_i^2 . In particular Eq. 22 highlights the conditions for which the density will be uniform, i.e., $g = 0$. Previously, the density was uniform if the neural population variances were equal, $\sigma_e^2 = \sigma_i^2$ [30, 15]. However, by introducing sparsity the condition for a uniform spectral density ($g = 0$) is much more specific. It requires that sparse population variances be equal $\sigma_{ke}^2 = \sigma_{ki}^2$. This implies that the simplest solution ($g = 0$) is equal population means $|\mu_e| = |\mu_i|$, and equal population variances $\sigma_e^2 = \sigma_i^2$.

We reformulate the expression for the spectral density such that the formula is symmetric with respect to the two variances. Let $P_{sk} = \frac{1}{\sigma_{sk}^2}$ for $k = e, i$ be the precision of the excitatory and inhibitory weight distributions, respectively. Hence we define the spectral density in terms of the sum of the precisions, $\Sigma P = P_{se} + P_{si}$, the difference in the precisions, $\Delta P = P_{se} - P_{si}$, and the difference of proportions, $\Delta f = 2f - 1$, as

$$\rho(z) = \begin{cases} \frac{1}{2\pi N} [\Sigma P - \Delta P \mathcal{H}_{\Delta f} (\Delta P |z|^2)] & |z| \leq \mathcal{R} \\ 0 & |z| > \mathcal{R} \end{cases} \quad (24)$$

where,

$$\mathcal{H}_{\Delta f}(x) = \frac{x - \Delta f N}{\sqrt{(x - \Delta f N)^2 + N^2(1 - \Delta f^2)}}. \quad (25)$$

The differences in precisions ΣP and proportion Δf can be switched around to favour inhibition, and the expression is equivalent. This new formulation emphasises that the non-uniformity is linked to the $|z|^2$ term, which is paired only with the difference in the precisions ΔP . Therefore, it is ΔP , that cause the non-uniform spectral density. By definition ΔP depends on the sparsity parameter, and the mean and variance of the excitatory and inhibitory weights, and hence so does the spectral density. This reformulation gives a detailed insight into the interaction of the statistics with the density of eigenvalues across the disc.

3.3.2 Local eigenvalue-outliers: a new zero row-sum (ZRS) condition

We observe a small number of eigenvalues escaping the compact circular support in the form of local eigenvalue-outliers crossing the theoretical radius. These eigenvalue crossings have been studied by Rajan et al. [30] and Tao [36], for fully connected matrices obeying Dale's law, and we extend the analysis here to the sparse unbalanced case.

This phenomena is illustrated in Figure 2. Figure 2(b) shows that there exists a small deviation between the numerically estimated radius (black dots) and the hypothesised eigenspectral-disc radius (coloured lines). The small difference between the two estimates is due to a handful of eigenvalues escaping the eigenspectral-disc compact support radius, as seen in Figure 2(a). Further, Figure 2(c) illustrates that the density of eigenvalues does not drop off as precisely in the numerical estimate as it does in the analytical calculation of the density, Eq. 21 and Eq. 22. This

highlights that the crossing magnitude of these eigenvalue-outliers is relatively small, and that the magnitude of the crossings increase as α approaches 1. The phenomena was first identified in previous studies for fully connected random matrices obeying Dale's law [30, 36, 15].

These papers define a projection operator to ensure that the row-sum of the random component of the synaptic connectivity matrix is zero, referred to as the zero row sum (ZRS) condition. This ensures that in the thermodynamic limit all eigenvalues converge to lie inside the compact support radius. The ZRS condition, which is equivalent to the row sum condition outlined in Eq. 3, is defined as,

$$\sum_{j=1}^N J_{ij} = 0, \quad (26)$$

where J_{ij} are the entries in the random component $J = AD$ of the connectivity weight matrix W .

For fully connected random matrices obeying Dale's law, the ZRS condition is implemented through the use of a projection operator P that is defined in [36, 30, 15] and takes the form

$$P = \mathbb{1}_N - \frac{uu^\top}{N}, \quad (27)$$

with $u = (1, \dots, 1)^\top$. The operator P is used such that the synaptic connectivity matrix takes the form,

$$W = ADP + uv^\top. \quad (28)$$

Here we aim to construct an analogous implementation of the ZRS condition, namely a sparse zero row-sum condition (SZRS) for sparse matrices that obey Dale's law. We hypothesise that the constraint will ensure that all eigenvalues lie within the compact support radius in the thermodynamic limit. A potential solution would be to derive an analogous projection operator to ensure the rows of the random component J sum to zero. However, due to the nature of matrix multiplication, such an operator will not preserve the sparsity pattern. To ensure the sparsity pattern is preserved we instead enforce a zero row-sum by subtracting the average of the rows from each nonzero entry from the random component $J = S \circ AD$ of the connectivity matrix W . This is succinctly defined as;

$$W = (J - B) + S \circ uv^\top; \quad (29)$$

where $B_{ij} = S_{ij}\bar{J}_i$ and the average of the row $\bar{J}_i = \sum_j J_{ij} / \sum_j S_{ij}$.

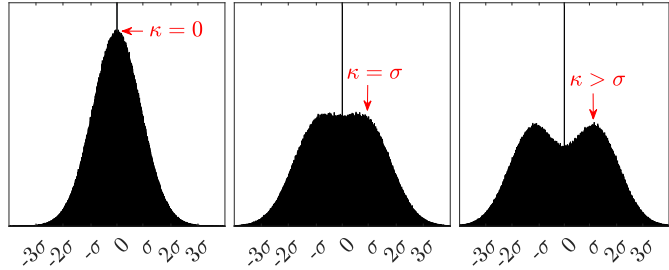
The SZRS condition enforces a zero row-sum and strictly preserves the sparsity pattern specific to the realisation of W . This implementation of the ZRS condition is equivalent to the original condition, Eq. 26 introduced in [30, 36, 15] when the matrix is fully connected. If the ZRS or SZRS condition is applied, then fewer eigenvalues cross the eigenspectral-disc radius than if no row-sum constraint is applied. However, the condition does not ensure all eigenvalues will lie within the eigenspectral-disc radius in the thermodynamic limit, Figure 3. In the next section we explore this phenomenon further by constructing a numerical homotopy to examine how sparsity and Dale's law effect eigenvalue crossings of the eigenspectral-disc compact support radius when the SZRS condition is satisfied.

3.3.3 A homotopy analysis of the breakdown of the row-sum condition

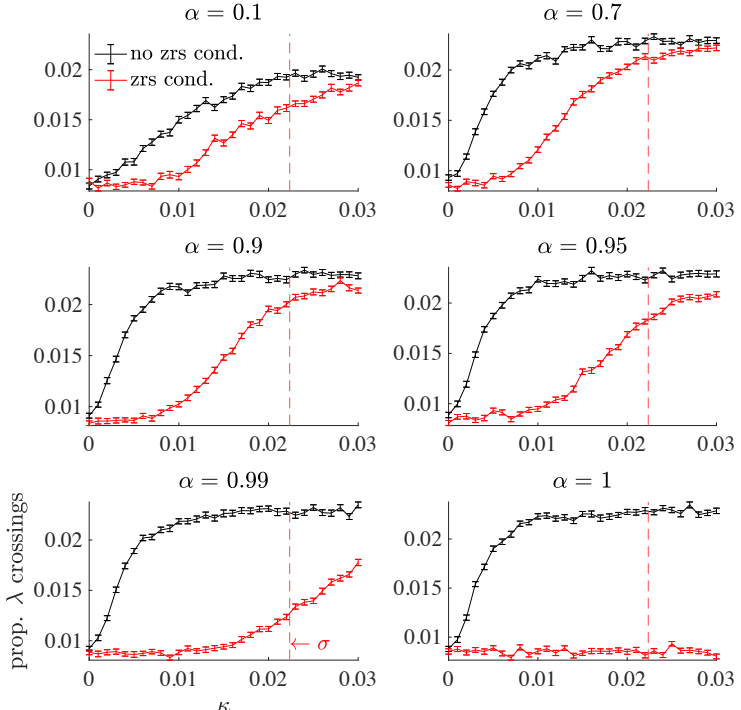
In non-sparse random synaptic connectivity matrices obeying Dale's law, it is the separation of the means of the two neural distributions that cause eigenvalues to cross the eigenspectral-disc radius [30, 36]. We propose that a similar result holds for sparse balanced and unbalanced random matrices obeying Dale's law. To investigate the effects of sparsity and Dale's law, we perform a numerical homotopic mapping. A homotopy is a continuous (but not necessarily homeomorphic) mapping from one limiting case to another limiting case. For example, $H = \kappa F + (1 - \kappa)G$ such that $H: G \mapsto F$ as κ goes from $0 \rightarrow 1$, where κ is the homotopy parameter [29]. Specifically, we map how the excitatory and inhibitory neural distributions deform from a single Gaussian distribution ($\mu = \kappa = 0, \sigma = 1/\sqrt{N}$) into two distinct Gaussian distributions with means $\mu_e = \kappa$, and $\mu_i = -\kappa$ and identical variances $\sigma_e^2 = \sigma_i^2 = 1/\sqrt{N} = \sigma$. This linear homotopic mapping will show that as the excitatory and inhibitory distributions separate, the proportion of eigenvalues that cross the theoretical eigenvalue disc radius increase. We perform the homotopic mapping for two cases, connectivity matrices that satisfy the SZRS condition, and connectivity matrices that do not satisfy the SZRS condition. We hypothesise that, similar to the ZRS condition, the SZRS condition will ensure fewer eigenvalues cross the disc as the two distributions separate.

The order parameter of the homotopy is κ , and defines the degree of separation of the means of the two neural distributions. The numerical homotopy, Figure 3 and Figure 6 in the Appendix, illustrates how this degree of separation, κ , affects the proportion of eigenvalue crossings for both sparse and non-sparse ($\alpha = 1$) matrices. Figure 3(b) plots the proportion of eigenvalue crossings that are calculated and averaged over 100 realisations for matrices that have implemented both SZRS condition implemented (red) and no condition implemented (black). The proportion of eigenvalue crossings are close to but not equal to zero due to finite size effects, and numerical estimation of eigenvalues. A similar Figure is shown in the appendix for an unbalanced case Figure 6.

When $\kappa = 0$ the entries w_{ij} of the connectivity matrix form a single Gaussian distribution with a large peak at zero due to the binomial distribution of the sparsity matrix S , Figure 3(a). The peak at zero changes only with the



(a)



(b)

Figure 3: Numerical homotopy illustrating the average proportion of eigenvalue crossings as a function of the continuous deformation of a single Gaussian distribution ($\kappa = 0$), with binomial peak from sparsity, to two distinct Gaussian distributions $\kappa = \sigma$, also with a binomial peak. The proportion is an average calculated over 100 realisations, and the standard error is included as bars on each point. The homotopy parameter κ controls the separation of the means of the two populations, $\mu_e = \kappa$, $\mu_i = -\kappa$, and the population variances are identical $\sigma_e^2 = \sigma_i^2 = 1/N = \sigma^2$. The matrix has dimension $N = 2000$ and $f = 0.5$. Each sub-figure shows the homotopy for different values of α .

sparsity parameter α . As κ increases the Gaussian distribution widens, continuously deforming one population into two populations. We observe that for low degrees of distribution separation $\kappa \ll \sigma$, the zero-row sum condition works most optimally to ensure few eigenvalues cross the eigenspectral-disc radius. Moreover, we find that the zero-row sum condition works better for $\kappa \ll \sigma$ when the matrix is closer to being fully connected, $\alpha > 0.9$.

As $\kappa \rightarrow 1$ the single Gaussian distribution separates into two distinct Gaussian peaks, with a large peak at zero due to sparsity. At this point the means of the excitatory/inhibitory populations are significantly different, i.e., two standard deviations of separation, thus Dale's law is effectively implemented in the network connectivity, Figure 3(a). When $\kappa = \sigma$, the numerical homotopy shows the breakdown of the ability of the SZRS condition to ensure all eigenvalues lie inside the circular support of the eigenspectrum. This breakdown is evident even in the $\alpha \rightarrow 1$ limit. When the network is fully connected, we observe that the zero row sum effectively ensures that the majority of eigenvalues lie within the eigenspectral-disc compact support radius. However, as soon as a small amount of sparsity is introduced (see Figure 3(b): $\alpha = 0.99$), the SZRS condition ensures only that fewer eigenvalues escape the circular support. The numerical homotopy analysis illustrates that though the SZRS condition works to prevent fewer local eigenvalue-outliers, the condition does not ensure the removal of all local eigenvalue-outliers in the sparse case.

4 Discussion

In this paper we examined the stability of random neural networks with more realistic anatomical structures in the form of sparse connectivity and Dale's law. Specifically, we examined the eigenspectrum of the associated network Jacobian for sparse (un)balanced random synaptic connectivity matrices obeying Dale's law. The results presented here consider all levels of network sparseness $0 \leq \alpha \leq 1$, and also implements Dale's law using distributed weights. Therefore, the expressions derived significantly extend previous studies which only separately consider (i) fully connected random matrices obeying Dale's law [30, 15], (ii) one population sparse random matrices with zero mean [37, 14], or (iii) sparse matrices (in the sparse limit $\alpha \ll 1$) with constant weights describing each of the excitatory and inhibitory populations [26, 22].

4.1 The eigenvalue outlier and eigenspectral-disc radius.

The eigenspectrum of the network Jacobian evaluated at the homogeneous equilibrium, consists of an eigenvalue outlier λ_O (for the unbalanced case), and a eigenspectral-disc with radius \mathcal{R} . Here, we derived functions of the statistics of the synaptic weights to predict these quantities. Our results show that the location of the eigenvalue outlier is linearly related to the sparsity parameter (α), and structural (E-I) (im)balance. Interestingly, we show that the variance of the connectivity matrix and consequently the radius of the eigenspectral-disc scales non-linearly with the sparsity parameter, the both population means and variances (Eq. 20 and Figure 1(b)).

The analytical expressions, Eq. (10, 19) were used to predict the eigenvalue outlier, and eigenspectral-disc radius for a large number of realisations of sparse (un)balanced random matrices that obey Dale's law. The results (Figure 2) show that the expressions for the eigenvalue outlier, Eq. (10, 19), and radius of the eigenspectral-disc, Eq. (12, 20) accurately and precisely predict the outlier value and eigenspectral-disc radius for matrices of this form.

4.2 Eigenspectral density

Our results also demonstrate that introducing sparsity to a network of distinct excitatory and inhibitory neural populations changes the spectral density to become non-uniform, even when the population variances are the same. Previous spectral density results are extended in this paper, by incorporating the new expressions for the sparse variances of the excitatory and inhibitory weights, Eq. 18, into the previously derived spectral density formula Eq. (21, 22) defined in [30, 15].

We further revised the spectral density formula such that the expression is symmetric with respect to the statistics of the excitatory and inhibitory weights. Our reformulation, Eq. 24, is written in terms of the precision and emphasises that the non-uniform spectral density is dependent on the difference of the precisions, ΔP . This formulation highlights that non-uniform density depends on not only the difference in the population variances $\sigma_e^2 \neq \sigma_i^2$, but also the difference in the magnitude of the population means $|\mu_e| \neq |\mu_i|$. This additional requirement is counter-intuitive due to the nonlinear interaction between sparsity α and the population means when $\alpha \neq 1$. Furthermore, if we extend this analysis and define population specific sparsity parameters α_e, α_i , then the non-uniform spectral density further depends on this difference as well. The finding is important, because it shows an intricate interplay of all of the statistics, rather than just between the variances of the excitatory and inhibitory weights as shown previously [30, 15].

4.3 Identifying local outliers, and deriving a new ZRSC

We observed for sparse random matrices obeying Dale's law that a small number of local-eigenvalue-outliers escape the eigenvalue spectral disc radius, as shown in Figure 2. This is a result consistent with fully connected random matrices also obeying Dale's law [30, 36, 15]. Previous studies derive a projection operator for the fully connected case to enforce a zero-row sum, Eq. (26, 27) and therefore ensure that these local eigenvalues converge to lie within the eigenvalue spectral disc radius in the thermodynamic limit. Such a projection operator does not work for the sparse case as the sparsity pattern will not be preserved. Therefore, we implemented an analogous condition for sparse random matrices obeying Dale's law, Eq. 29, that does ensure that the ZRS condition is satisfied. Unlike in the fully connected case, this condition ensures only that fewer eigenvalues escape the eigenspectrum-disc radius in the thermodynamic limit. We conjecture that this is due to the interaction of the sparse binomial distribution with the two distinct Gaussian distributions of the neural populations, which we speculate maybe generated by a different point process than for the fully connected case [36].

4.4 Construction of numerical homotopic mapping

We further investigated the non-convergence of the local eigenvalue outliers to lie within the eigenspectrum-disc by constructing a numerical homotopy to prove that the ZRS condition breaks down. The two interrelated causes of the breakdown are the incorporation of sparsity, and Dale's law into the connectivity matrix. Our result indicates that even a small divergence from a fully connected random matrix obeying Dale's law introduces local eigenvalue-outliers that can no longer be removed by a ZRS condition. This result holds for both structural (E-I) balanced, and unbalanced matrices.

4.5 Interaction of sparsity with structural E-I balance

Our results show that there exists a fundamental interplay between sparsity, the population means and variances in the prediction of key eigenspectral distribution properties. When Dale's law is implemented in sparse random matrices, the structural (E-I) balance linearly scales with the sparsity parameter α , Eq. 15. However, introducing sparsity changes both the variances of the excitatory and inhibitory weights $\sigma_{sk}^2, (k = e, i)$, and the overall variance of the matrix W , $\text{Var}(w_{ij})$. This in turn non-linearly scales the radius of the eigenvalue spectral disc and spectral density across the disc. The radius is dependent on the non-linear interaction between the sparsity parameter, α , the square of the population means μ_e^2, μ_i^2 , and population variance σ_e^2, σ_i^2 , Eq. 20. Therefore, unless $\alpha = 1$ and / or $\mu_e = \mu_i = 0$, the radius depends on the population means in addition to the variances as previously noted in [30, 15]. Interestingly, if the matrix is structurally E-I balanced, i.e., Eq. 15 is zero, the radius of the eigenspectral disc still scales as a function of the sparsity parameter, the population means and variances (see Figure 4(b) in Appendix).

The spectral density is dependent on the differences between the sparse population variances, Eq. (21,22), which are non-linearly dependent on the sparsity parameter and the means and variances of both the excitatory and inhibitory populations. The eigenvalue spectral density can be non-uniform even if the network is structurally E-I balanced and the population variances σ_e^2, σ_i^2 are equal. This is due to the dependency of the variances, Eq. 16 of the excitatory and inhibitory weights on the square of the means μ_e^2, μ_i^2 . The analysis presented in this paper is straightforwardly extendable to distinct sparsity parameters for each neural population, i.e., $\alpha_e \neq \alpha_i$. We find that this distinction has further implications on the structural E-I balance and hence the eigenvalue outlier, the spectral disc radius, and the spectral density.

4.6 Implications on neural network dynamics

Our results provide insight into what combination of factors contribute to the stability of large networks of neurons and other complex networked dynamical systems [2]. Regulating neural function, and dynamic E-I balance must take into account network sparsity at all levels of network connectedness. By examining the eigenspectra of sparse random matrices obeying Dale's law we find that though the eigenspectra are similar to those in their fully connected counterparts [30], there are a few key differences that influence the stability, and therefore the transition into spontaneous asynchronous activity.

4.6.1 Inducing non-trivial dynamics

As discussed previously, non-trivial spontaneous asynchronous activity occurs when the eigenspectral-disc crosses the stability boundary. This can happen via the interplay between the time-constant, τ , (which positions the disc centre) and the variance of the connectivity matrix (which determines the radius of the eigenspectral disc) [15]. However, for sparse unbalanced random matrices obeying Dale's law this interplay is more complex.

If the sparse network obeying Dale's law is excitatory dominated, i.e., $\alpha(f\mu_e + (1-f)\mu_i) > 0$, then the eigenvalue outlier crosses the stability boundary. Destabilisation occurs if the real part of the largest eigenvalue, the eigenvalue outlier λ_O is greater than zero. If, however the sparse network is balanced, or inhibitory dominated, $\alpha(f\mu_e + (1-f)\mu_i) \leq 0$, non-trivial dynamics are first induced by the radius of the eigenspectral-disc crossing the stability boundary. Previous studies found that the transition is induced solely by the interplay between the membrane time constant and the population variances [30, 22, 15]. We find that for structural (E-I) balanced and inhibitory dominated networks, the relationship is significantly more complex than found previously. Specifically, the transition depends on the interaction between the membrane time constant, the sparsity parameter, the population means, and the population variances.

Furthermore, the non-uniform eigenspectral density ensures that more eigenvalues lie near the centre of the disc and fewer eigenvalues lie near the edge. This means that there are fewer eigenvalues that lie adjacent to the stability boundary (and fewer on the other side of the disc), generating less complex and more structured dynamics than seen from a purely random matrix.

4.6.2 Local eigenvalue outliers influencing destabilisation and non-trivial dynamics

In the case of sparse inhibitory dominated matrices obeying Dale's law, destabilisation may not be predicted accurately by the radius, \mathcal{R} , due to local eigenvalue-outliers crossing the radius of the eigenspectral-disc. Our analysis shows that these local eigenvalue-outliers introduced by sparsity and Dale's law are unable to be constrained to lie within the eigenspectral-disc disc through a ZRS condition, and it is currently unclear how to derive an appropriate condition to constrain these eigenvalues.

The ZRS condition acts on the random component of the connectivity matrix, and ensures every row in the connectivity matrix W has a constant sum, Eq. 3. If the connectivity matrix has structural (E-I) balance then the ZRS condition enforces a 'tight' neuron-to-neuron input balance, and the network operates under balanced input conditions, i.e., dynamic balance, [15, 4, 18, 1]. Contrary to this, if the connectivity matrix is structurally (E-I) unbalanced then the ZRS condition does not enforce a neuron-to-neuron balance, and the network functions in either an excitatory/inhibitory dominated regime. These regimes are thought to provide substrates for pathological dynamics to emerge, such as pathological oscillations seen in seizures [4, 19, 15].

4.7 Limitations and future research

The analysis presented in this paper examines the local stability of the network around the homogeneous equilibrium in the asymptotic limit. Therefore, this investigation yields insight into the transition to spontaneous activity, but the exact nature of such dynamics after the transition is not able to be analysed within this framework. Further, as discussed our analysis only strictly applies to homogeneous equilibria. Heterogeneous equilibrium solutions are dependent on the realisation of the synaptic connectivity matrix, so an additional dependency is introduced to the networked Jacobian. Specifically, the Jacobian, Eq. 5 may no longer be statistically proportional to the connectivity matrix, W , diagonally offset by $-1/\tau$, as the matrix $\Phi'(\mathbf{x}^*)$ can be heterogeneous and will influence the statistics of the networked Jacobian. The analysis framework we present is applicable to heterogeneous fixed points and different firing-rate functions as shown numerically in [26, 22]. However, it is unclear how heterogeneous the matrix $\Phi'(\mathbf{x}^*)$ has to be before it influences the statistics of the networked Jacobian and the results from random matrix theory no longer apply.

Another limitation of the network model used here is the assumption of instantaneous rise time in the post-synaptic potentials, i.e., there is no synaptic dynamics. A possible future extension is to incorporate synaptic dynamics, such as through the introduction of conductance-based synapses [28]. Modelling synaptic dynamics is more realistic and could significantly change the dynamics through the additional feedback non-linearity. However, even though the network model used in this paper is not physiologically detailed, significant insight is generated about the neural system it describes, particularly in regards to the relationship between connectivity and dynamics.

Furthermore, we examine randomly distributed connectivity weights that follow the product distribution of binomial and Gaussian random variables. However, connectivity weights in the cortex have been found to be log-normally distributed [9]. As this work is based on results from random matrix theory, which hold for any iid random variable [37], the results presented here should be extendable for any iid random variable, including log-normal random variables.

The analysis presented here is performed for general ratios and distributions of excitation to inhibition, and probability of connection α . For a local cortical network the typical ratio of number of excitatory to inhibitory connections is 4:1 [6, 17, 32]. Therefore, for structural (E-I) balance the strength of inhibition (i.e., the number of inhibitory synapses times their amplitude) must be four times that of excitation. A direct application of this analysis is to examine the connectivities of a local cortical network constructed with key statistics extracted from large connectomic data sets [16, 27, 31]. The statistics pertain to the ratio of inhibition to excitation, the mean and variance of the excitatory and inhibitory connections, and the average number of connections of a neuron to other neurons (sparsity). We further note that synaptic self-connections (autapses), are not very common [3, 5]. However, we do not eliminate the self connection terms (diagonal terms) in the connectivity matrix, as the effect of removing these is negligible for large N . For finite sized networks, this should be a consideration particularly with analysis using connectomic data statistics.

4.8 Conclusion

In conclusion, network sparsity and Dale’s law are two fundamental anatomical properties of local cortical networks in the brain. The respective impacts of these properties have been previously individually examined. This paper analyses their combined influences for structurally E-I balanced and unbalanced networks and demonstrates that balance and sparsity interact in ways that have not previously been studied. We show that sparsity linearly scales the structural E-I balance of a connectivity matrix, and the eigenvalue outlier. However, in contrast to this, the variance of the connectivity matrix is a function of the nonlinear interaction between sparsity and the population means and variances. Therefore, the eigenvalue spectral disc radius also scales in this nonlinear fashion. Further, we find that the nonlinear interaction of sparsity with the population means and variances also influences the non-uniform eigenvalue spectral density. Our final result numerically demonstrates that for sparse balanced and unbalanced random matrices obeying Dale’s law, the zero row sum condition does not ensure all eigenvalues converge to lie within the eigenspectral-disc. Therefore, our results indicates that there is a dynamical and non-linear interplay between network sparsity and all the E-I population statistics that is fundamental to regulating neural network dynamics.

The analysis presented here further develops the quantitative relationship between neural network architectures and neural dynamics. This relationship is of particular importance for both theoretical and experimental neuroscience with the promise of a plethora of connectome data in the near future. Our results are an important step towards developing analysis techniques that will be essential to understand and elucidate how connectome statistics impact on neural network dynamics.

References

- [1] Yashar Ahmadian and Kenneth D Miller. “What is the dynamical regime of cerebral cortex?” In: *Neuron* 109.21 (2021), pp. 3373–3391.
- [2] Stefano Allesina and Si Tang. “The stability–complexity relationship at age 40: a random matrix perspective”. In: *Population Ecology* 57.1 (2015), pp. 63–75.
- [3] Alberto Bacci and John R Huguenard. “Enhancement of spike-timing precision by autaptic transmission in neocortical inhibitory interneurons”. In: *Neuron* 49.1 (2006), pp. 119–130.
- [4] Jérémie Barral and Alex D Reyes. “Synaptic scaling rule preserves excitatory–inhibitory balance and salient neuronal network dynamics”. In: *Nature neuroscience* 19.12 (2016), pp. 1690–1696.
- [5] John M Bekkers. “Synaptic transmission: functional autapses in the cortex”. In: *Current Biology* 13.11 (2003), R433–R435.
- [6] Valentino Braitenberg and Almut Schüz. *Anatomy of the cortex: statistics and geometry*. Vol. 18. Springer Science & Business Media, 2013.
- [7] Nicolas Brunel. “Dynamics of sparsely connected networks of excitatory and inhibitory spiking neurons”. In: *Journal of computational neuroscience* 8.3 (2000), pp. 183–208.
- [8] Nicolas Brunel and Xiao-Jing Wang. “What determines the frequency of fast network oscillations with irregular neural discharges? I. Synaptic dynamics and excitation-inhibition balance”. In: *Journal of neurophysiology* 90.1 (2003), pp. 415–430.
- [9] György Buzsáki and Kenji Mizuseki. “The log-dynamic brain: how skewed distributions affect network operations”. In: *Nature Reviews Neuroscience* 15.4 (2014), pp. 264–278.
- [10] John Carew Eccles. “From electrical to chemical transmission in the central nervous system: the closing address of the sir henry dale centennial symposium cambridge, 19 september 1975”. In: *Notes and records of the Royal Society of London* 30.2 (1976), pp. 219–230.
- [11] Vyacheslav L Girko. “Circular law”. In: *Theory of Probability & Its Applications* 29.4 (1985), pp. 694–706.
- [12] David Golomb and David Hansel. “The number of synaptic inputs and the synchrony of large, sparse neuronal networks”. In: *Neural computation* 12.5 (2000), pp. 1095–1139.
- [13] Srinivas Gorur-Shandilya et al. “Mapping circuit dynamics during function and dysfunction”. In: *Elife* 11 (2022), e76579.
- [14] Elizabeth Herbert and Srdjan Ostojic. “The impact of sparsity in low-rank recurrent neural networks”. In: *PLOS Computational Biology* 18.8 (Aug. 2022), pp. 1–21. doi: 10.1371/journal.pcbi.1010426. URL: <https://doi.org/10.1371/journal.pcbi.1010426>.
- [15] Jesper R Ipsen and Andre DH Peterson. “Consequences of Dale’s law on the stability-complexity relationship of random neural networks”. In: *Physical Review E* 101.5 (2020), p. 052412.
- [16] Allan R Jones, Caroline C Overly, and Susan M Sunkin. “The Allen brain atlas: 5 years and beyond”. In: *Nature Reviews Neuroscience* 10.11 (2009), pp. 821–828.
- [17] Eric R Kandel et al. *Principles of neural science*. Vol. 4. McGraw-hill New York, 2000.
- [18] Itamar D Landau and Haim Sompolinsky. “Macroscopic fluctuations emerge in balanced networks with incomplete recurrent alignment”. In: *Physical Review Research* 3.2 (2021), p. 023171.
- [19] Itamar Daniel Landau and Haim Sompolinsky. “Coherent chaos in a recurrent neural network with structured connectivity”. In: *PLoS computational biology* 14.12 (2018), e1006309.
- [20] Eve Marder and Jean-Marc Goaillard. “Variability, compensation and homeostasis in neuron and network function”. In: *Nature Reviews Neuroscience* 7.7 (2006), pp. 563–574.
- [21] Jorge Mariño et al. “Invariant computations in local cortical networks with balanced excitation and inhibition”. In: *Nature neuroscience* 8.2 (2005), pp. 194–201.
- [22] Francesca Mastrogiovanni and Srdjan Ostojic. “Intrinsically-generated fluctuating activity in excitatory-inhibitory networks”. In: *PLoS computational biology* 13.4 (2017), e1005498.
- [23] Francesca Mastrogiovanni and Srdjan Ostojic. “Linking connectivity, dynamics, and computations in low-rank recurrent neural networks”. In: *Neuron* 99.3 (2018), pp. 609–623.
- [24] Hamish Meffin, Anthony N Burkitt, and David B Grayden. “An analytical model for the ‘large, fluctuating synaptic conductance state’ typical of neocortical neurons in vivo”. In: *Journal of computational neuroscience* 16.2 (2004), pp. 159–175.
- [25] Madan Lal Mehta. *Random matrices*. Elsevier, 2004.
- [26] Srdjan Ostojic. “Two types of asynchronous activity in networks of excitatory and inhibitory spiking neurons”. In: *Nature neuroscience* 17.4 (2014), pp. 594–600.

[27] Casey Paquola et al. “The BigBrainWarp toolbox for integration of BigBrain 3D histology with multimodal neuroimaging”. In: *Elife* 10 (2021), e70119.

[28] Andre D. H. Peterson et al. “A homotopic mapping between current-based and conductance-based synapses in a mesoscopic neural model of epilepsy”. In: <https://arxiv.org/abs/1510.00427> (2015). doi: 10.48550/ARXIV.1510.00427. URL: <https://arxiv.org/abs/1510.00427>.

[29] Saeed Khaleghi Rahimian et al. “A new homotopy for seeking all real roots of a nonlinear equation”. In: *Computers & chemical engineering* 35.3 (2011), pp. 403–411.

[30] Kanaka Rajan and Larry F Abbott. “Eigenvalue spectra of random matrices for neural networks”. In: *Physical review letters* 97.18 (2006), p. 188104.

[31] Alexander Shapson-Coe et al. “A connectomic study of a petascale fragment of human cerebral cortex”. In: *BioRxiv* (2021).

[32] Gordon M Shepherd. *The synaptic organization of the brain*. Oxford university press, 2004.

[33] Haim Sompolinsky, Andrea Crisanti, and Hans-Jurgen Sommers. “Chaos in random neural networks”. In: *Physical review letters* 61.3 (1988), p. 259.

[34] Kevin Staley. “Molecular mechanisms of epilepsy”. In: *Nature neuroscience* 18.3 (2015), pp. 367–372.

[35] Merav Stern, Haim Sompolinsky, and Laurence F Abbott. “Dynamics of random neural networks with bistable units”. In: *Physical Review E* 90.6 (2014), p. 062710.

[36] Terence Tao. “Outliers in the spectrum of iid matrices with bounded rank perturbations”. In: *Probability Theory and Related Fields* 155.1 (2013), pp. 231–263.

[37] Terence Tao and Van Vu. “Random matrices: the circular law”. In: *Communications in Contemporary Mathematics* 10.02 (2008), pp. 261–307.

[38] Terence Tao, Van Vu, and Manjunath Krishnapur. “Random matrices: Universality of ESDs and the circular law”. In: *The Annals of Probability* 38.5 (2010), pp. 2023–2065.

[39] Carl Van Vreeswijk and Haim Sompolinsky. “Chaos in neuronal networks with balanced excitatory and inhibitory activity”. In: *Science* 274.5293 (1996), pp. 1724–1726.

[40] Gilles Wainrib and Jonathan Touboul. “Topological and dynamical complexity of random neural networks”. In: *Physical review letters* 110.11 (2013), p. 118101.

5 Appendix

5.1 Calculating the mean and variance of the entries of a sparse (un)balanced random matrix.

We calculate the expected value and variance of the entries in a sparse (un)balanced random matrix, W , as constructed in Eq. 8 with mean, μ and variance, σ^2 of the partially random component $\hat{W} = AD + M$, and sparse component S defined by the probability of connection α . The expected value of the entries in W takes the form

$$\begin{aligned}\mathbb{E}(w_{ij}) &= \frac{1}{N^2} \sum_{i=1}^N \sum_{j=1}^N w_{ij} \\ &= \frac{1}{N^2} \sum_{i=1}^N \sum_{j=1}^{(1-\alpha)N} 0 + \frac{1}{N^2} \sum_{i=1}^N \sum_{j=1}^{\alpha N} \hat{w}_{ij} \\ &= \alpha \mu.\end{aligned}\tag{30}$$

The variance takes the form

$$\begin{aligned}\mathbb{V}\text{ar}(w_{ij}) &= \frac{1}{N^2} \sum_{i=1}^N \sum_{j=1}^N w_{ij}^2 - \left(\frac{1}{N^2} \sum_{i=1}^N \sum_{j=1}^N w_{ij} \right)^2 \\ &= \frac{1}{N^2} \sum_{i=1}^N \sum_{j=1}^{(1-\alpha)N} 0^2 + \frac{1}{N^2} \sum_{i=1}^N \sum_{j=1}^{\alpha N} \hat{w}_{ij}^2 - \alpha^2 \mu^2 \\ &= \frac{1}{N^2} \sum_{i=1}^N \sum_{j=1}^{\alpha N} \hat{w}_{ij}^2 - \alpha^2 \mu^2 \\ &= \frac{1}{M} \sum_{k=1}^{\alpha M} m_k^2 - \alpha^2 \mu^2 \quad (M = N^2, m_k = \hat{w}_{i,j}) \\ &= \alpha \frac{1}{\alpha M} \sum_{k=1}^{\alpha M} m_k^2 - \alpha^2 \mu^2 \\ &= \alpha (\mu^2 + \sigma^2) - \alpha^2 \mu^2\end{aligned}\tag{31}$$

Note that $\frac{1}{\alpha M} \sum_{k=1}^{\alpha M} m_k^2$ is the second non-central moment of $\mathcal{N}(\mu, \sigma)$. Hence, the expressions for $\mathbb{E}(w_{ij})$ and $\mathbb{V}\text{ar}(w_{ij})$ are

$$\mathbb{E}(w_{ij}) = \alpha \mu\tag{32}$$

$$\mathbb{V}\text{ar}(w_{ij}) = \alpha (\mu^2 + \sigma^2) - \alpha^2 \mu^2\tag{33}$$

5.2 Calculating the mean and variance of the entries of a sparse random matrix obeying Dale's law.

We commence by separately calculating the means of the excitatory and inhibitory weights in W constructed as in Eq. 8.

$$\begin{aligned}\mathbb{E}(w_{ij})_e &= \frac{1}{fN^2} \sum_{i=1}^N \sum_{j=1}^{fN} w_{ij} \\ &= \frac{1}{fN^2} \sum_{i=1}^N \sum_{j=1}^{f(1-\alpha)N} 0 + \frac{1}{fN^2} \sum_{i=1}^N \sum_{j=1}^{f\alpha N} w_{ij} \\ &= \alpha \mu_e \\ \mathbb{E}(w_{ij})_i &= \frac{1}{(1-f)N^2} \sum_{i=1}^N \sum_{j=1}^{(1-f)N} w_{ij} \\ &= \frac{1}{(1-f)N^2} \sum_{i=1}^N \sum_{j=1}^{(1-f)(1-\alpha)N} 0 + \frac{1}{(1-f)N^2} \sum_{i=1}^N \sum_{j=1}^{(1-f)\alpha N} w_{ij} \\ &= \alpha \mu_i\end{aligned}\tag{34}$$

The mean of the entries in the matrix W is simply the weighted sum of the means of the excitatory and inhibitory weights. This is expressed as follows,

$$\mathbb{E}(W) = f\mu_{se} + (1 - f)\mu_{si} \quad (35)$$

where $\mu_{sk} = \alpha\mu_k$ are the means of the excitatory and inhibitory weights $k = e, i$.

We now calculate the variances for each neural population and we substitute the second non-central moment of the population distribution to obtain separate variance expressions for the excitatory and inhibitory weights.

$$\begin{aligned} \mathbb{V}\text{ar}(w_{ij})_e &= \frac{1}{fN^2} \sum_{i=1}^N \sum_{j=1}^{fN} w_{ij}^2 - \left(\frac{1}{fN^2} \sum_{i=1}^N \sum_{j=1}^{fN} w_{ij} \right)^2 \\ &= \frac{1}{fN^2} \sum_{i=1}^N \sum_{j=1}^{f(1-\alpha)N} 0^2 + \frac{1}{fN^2} \sum_{i=1}^N \sum_{j=1}^{f\alpha N} \hat{w}_{ij}^2 - \alpha^2 \mu_e^2 \\ &= \frac{1}{fM} \sum_{k=1}^{f\alpha M} m_k^2 - \alpha^2 \mu_e^2 \\ &= \alpha \frac{1}{f\alpha M} \sum_{k=1}^{f\alpha M} m_k^2 - \alpha^2 \mu_e^2 \\ &= \alpha (\mu_e^2 + \sigma_e^2) - \alpha^2 \mu_e^2 \end{aligned} \quad (36)$$

$$\begin{aligned} \mathbb{V}\text{ar}(w_{ij})_i &= \frac{1}{(1-f)N^2} \sum_{i=1}^N \sum_{j=1}^{(1-f)N} w_{ij}^2 - \left(\frac{1}{(1-f)N^2} \sum_{i=1}^N \sum_{j=1}^{(1-f)N} w_{ij} \right)^2 \\ &= \frac{1}{(1-f)N^2} \sum_{i=1}^N \sum_{j=1}^{(1-f)(1-\alpha)N} 0^2 + \frac{1}{(1-f)N^2} \sum_{i=1}^N \sum_{j=1}^{(1-f)\alpha N} \hat{w}_{ij}^2 - \alpha^2 \mu_i^2 \\ &= \frac{1}{(1-f)M} \sum_{k=1}^{(1-f)\alpha M} m_k^2 - \alpha^2 \mu_i^2 \\ &= \alpha \frac{1}{(1-f)\alpha M} \sum_{k=1}^{(1-f)\alpha M} m_k^2 - \alpha^2 \mu_i^2 \\ &= \alpha (\mu_i^2 + \sigma_i^2) - \alpha^2 \mu_i^2 \end{aligned} \quad (37)$$

The variance of the entries in the matrix W is the weighted sum of the variance of the excitatory and inhibitory weights. We express this as

$$\mathbb{V}\text{ar}(W) = f\sigma_{se}^2 + (1 - f)\sigma_{si}^2, \quad (38)$$

where $\sigma_{sk}^2 = \alpha(1 - \alpha)\mu_k^2 + \alpha\sigma_k^2$ are the variances of the excitatory and inhibitory weights $k = e, i$.

5.3 Additional Figures

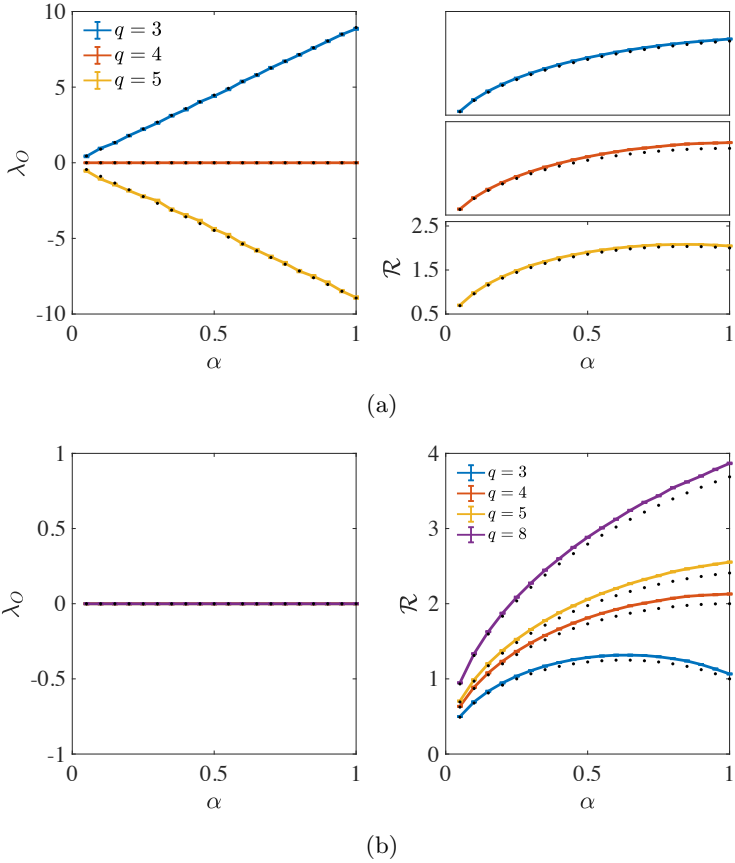


Figure 4: The eigenvalue outlier location and radius of the eigenspectral-disc for the matrix defined in Eq. 8, as a function of the sparsity probability α . (a) Illustrates the effects of holding the population variances, and excitatory mean constant and varying the inhibitory mean, and (b) the population means and excitatory variance is kept constant but the inhibitory variance is changed. The case the eigenvalue outlier is zero indicates a structurally E-I balanced network: orange in (a), and purple in (b). This is an extension to Figure 2(b). The theoretical outlier location and radius (blue, orange, yellow, purple) were calculated using definitions in Eq. 19 and 20, respectively. The largest λ_o and second largest eigenvalues λ_1 averaged over 100 realisations is shown in black. (a) Parameters of W are $N = 2000$, $f = 0.8$, $\mu_e = \frac{1}{\sqrt{N}}$, $\mu_i = -\frac{q}{\sqrt{N}}$, $\sigma_e = \sigma_i = \frac{1}{\sqrt{N}}$. (b) Parameters of W are $N = 2000$, $f = 0.8$, $\mu_e = \frac{1}{\sqrt{N}}$, $\mu_i = -\frac{4}{\sqrt{N}}$, $\sigma_e = \frac{1}{\sqrt{N}}$, $\sigma_i = \frac{q}{\sqrt{N}}$.

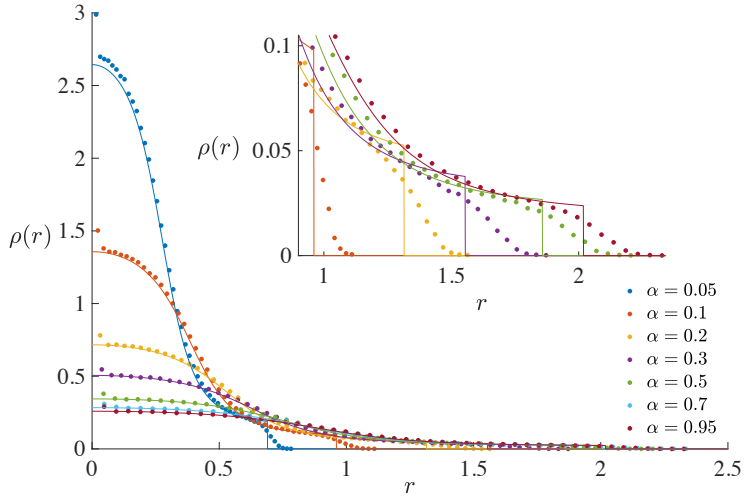


Figure 5: Non-uniform spectral density curves as a function of normalised disc radius and sparsity parameter α with analytical expression as solid lines and numerical simulations as points. This extends the results illustrated in Figure 2(c) to the structurally E-I unbalanced case. Parameters of W are $N = 2000$, $\mu_e = \frac{1}{\sqrt{N}}$, $\mu_i = -\frac{5}{\sqrt{N}}$, $\sigma_e = \frac{1}{\sqrt{N}}$, $\sigma_i = \frac{4}{\sqrt{N}}$, and $f = 0.8$.

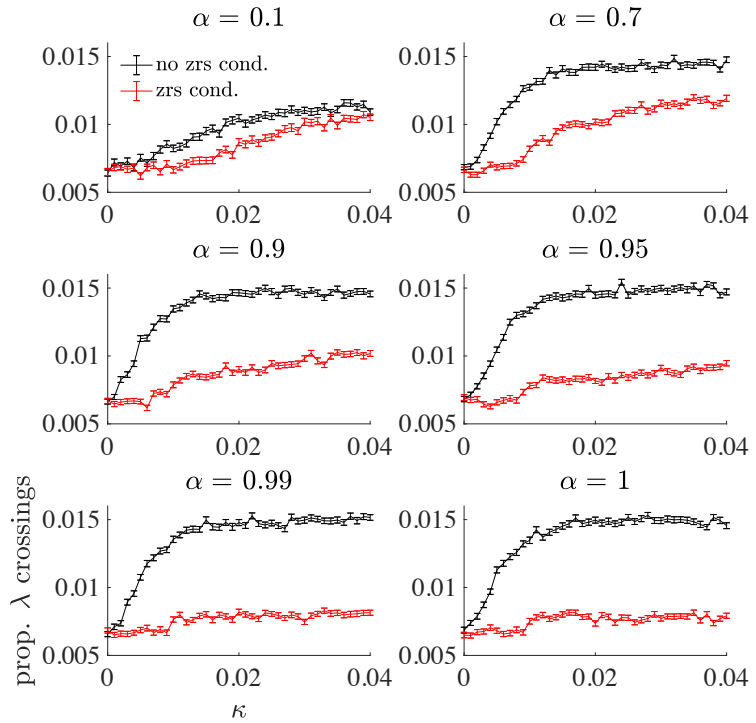


Figure 6: The homotopy continuation for the sparse unbalanced case. The proportion of eigenvalue crossings is an average calculated over $r = 250$ realisations, and the standard error is included as bars on each point. The homotopy parameter κ controls the separation of the means of the two populations, $\mu_e = \kappa$, $\mu_i = -5\kappa$, and the population variances are $\sigma_e^2 = 1/N$, $\sigma_i^2 = 4/N$. The matrix has dimension $N = 1000$ and the proportion of the excitatory population is $f = 0.8$. Each sub-figure shows the homotopy for different values of α where alpha ranges from 0.1 – 1.